Geophysical Journal International

Geophys. J. Int. (2013) **193,** 650–663 doi: 10.1093/gji/ggt012

Palaeomagnetic re-investigation of Early Permian rift basalts from the Baoshan Block, SW China: constraints on the site-of-origin of the Gondwana-derived eastern Cimmerian terranes

Jason R. Ali,[1] Haz M. C. Cheung,[1] Jonathan C. Aitchison[2] and Yadong Sun[3,4]

[1]*Department of Earth Sciences, University of Hong Kong, Pokfulam Road, Hong Kong, China. E-mail: jrali@hku.hk*
[2]*School of Geosciences, University of Sydney, Sydney, NSW* 2006*, Australia*
[3]*Faculty of Earth Sciences, China University of Geosciences, Wuhan, Hubei* 430074*, P. R. China*
[4]*School of Earth and Environment, University of Leeds, Leeds* LS2 9JT*, United Kingdom*

Accepted 2013 January 14. Received 2013 January 14; in original form 2012 May 10

SUMMARY

A palaeomagnetic investigation was carried out on a series of rift basalts (Woniusi Formation) that accumulated on the Baoshan block (SW China) in the Early Permian, the aim being to provide quantitative palaeogeographical information on the eastern Cimmerian terrane as it detached from eastern Gondwana. Reliable data were obtained from four locations/28 individual cooling units, and when combined with the findings of an earlier study (three locations/19 sites) indicate that breakup occurred at 41.9°S (with errors, 34.2–51.2°S). Using this information, we fit Baoshan against Gondwana within a narrow longitudinal belt close to where northeast Greater India and northwest Australia were once in close proximity. Furthermore, we suggest that Sibumasu (Simao-Burma-Malyasia-Sumatra; the largest of the eastern Cimmerian blocks) lay directly to the east, offshore of Australia; Qiangtang and Lhasa almost certainly sat to the west (off northern Greater India–SE Arabia), but we are uncertain as to their exact configuration. Our findings are compared with several rather different models that have been published in recent years. The new palaeomagnetic constraint highlights the flexibility authors currently have in reconstructing the region, principally because of the overall lack of similar high-quality data from the various blocks. We explain how new data could resolve these ambiguities, thereby offering more robust explanations for eastern Gondwana's late Palaeozoic development.

Key words: Palaeomagnetism applied to tectonics; Continental margins: divergent; Asia.

1 INTRODUCTION

Although there is a tendency to look upon continental breakup as involving the separation of large crustal entities (e.g. Africa–North America, Antarctica–Australia) a number of rifted margins have developed as a result of narrow slivers peeling from a 'mother' block. Examples include the Lord Howe Rise–Norfolk Ridge off eastern Australia in the Late Cretaceous, which formed the Tasman Sea basin, and the Palawan block from southern China in the mid-Cenozoic that created the South China Sea. Perhaps the most spectacular case of a sliver-block rifting is the Cimmerian terrane, which detached from eastern Gondwana in the Late Palaeozoic. Remnants of Cimmeria are present in an almost continuous belt stretching ∼13 800 km, from central Italy to east of Sumatra (Indonesia), via Greece, Turkey, Iran, Afghanistan, Tibet, SW China, Myanmar and Thailand (Fig. 1; Şengör *et al.* 1988; Stampfli *et al.* 2001; Moix *et al.* 2008; Metcalfe 2011). As a consequence of its vast length, an intriguing issue concerns exactly how the terrane, particularly the eastern portion, once abutted Gondwana. For many years, efforts to address this were biolithostratigraphically based (e.g. Wopfner 1996; Yan & Yin 2000; Ueno 2003). Recently, though, a number of teams have undertaken zircon age-dating of either basement rocks (e.g. Guynn *et al.* 2012) or critical clastic units (e.g. Gehrels *et al.* 2011; Zhu *et al.* 2011, 2013), the aim being to identify potential equivalents/source areas on the major Gondwana blocks. Interestingly, the data have resulted in reconstructions that are somewhat different to models that many would consider 'well-established'; *cf.* Guynn *et al.* (2012, fig. 9) and Zhu *et al.* (2013, fig. 7) with Metcalfe (1998, fig. 7) or Metcalfe (2002, fig. 9). Curiously, the one technique that might provide quantitative positioning data, palaeomagnetism, has not been applied in a systematic way to the Cimmerian terrane's eastern blocks. In an effort to rectify this, we report a study carried out on a basaltic series that was erupted across substantial parts of the Baoshan subterrane in southwest China (western Yunnan) as it detached from Gondwana in the mid-Early Permian.

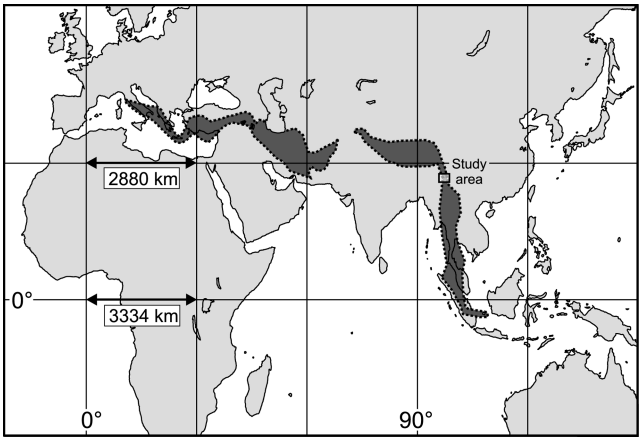

Figure 1. Map of a large part of the Eastern Hemisphere showing the Cimmerian terrane(s); projection is Gall-Peters. Based on Şengör *et al.* (1988), Stampfli *et al.* (2001), Moix *et al.* (2008) and Metcalfe (2011), the unit is shown in dark grey. The latitude/longitude markers have 30° spacings, inset box indicates the study area (Fig. 2).

2 GEOLOGICAL BACKGROUND

The fault-bounded Baoshan block is located in western Yunnan province, southwest China, adjacent to northeast Myanmar (Fig. 2). It is part of a collage of small and medium-size terranes (e.g. Qamdo–Simao, Linchang arc, West Burma) and larger crustal blocks (Indochina; Metcalfe 2002, 2011) that accreted to western South China during the Mesozoic. The Cenozoic arrival of India (Molnar & Tapponnier 1975; Patriat & Achache 1984; Jaeger *et al.* 1989; Aitchison *et al.* 2007), and the subsequent 'extrusion tectonics' (Tapponnier *et al.* 1982), has added an extra level of complexity with strike-slip faults, and to a lesser extent thrusts, 're-shuffling the deck' by displacing various crustal elements tens to several hundreds of kilometres to the southeast (Leloup *et al.* 1995; Wang *et al.* 1998; Ali *et al.* 2010; Fig. 1).

As with all of the Cimmerian blocks in southern and SE Asia (Wopfner 1996; Ridd 2009; Wopfner & Jin 2009; Metcalfe 2011),

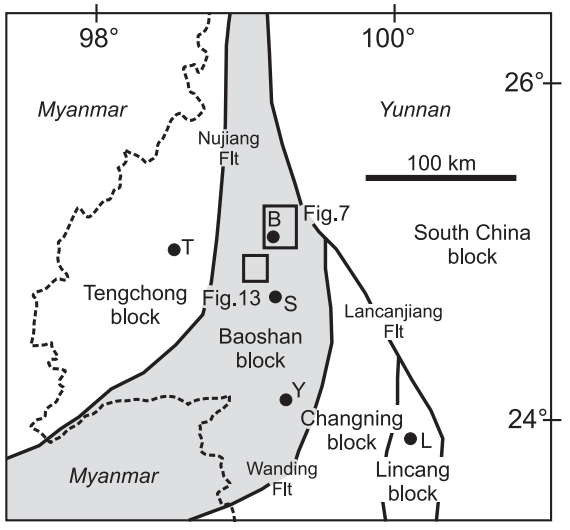

Figure 2. Map showing the regional tectonic relationships of the Baoshan block (shaded grey) together with the sampling areas. Abbreviations for cities/towns: B, Baoshan; L, Lincang; S, Shidian; Tengchong; Y, Yongde. Dashed line is the Myanmar–Yunnan (China) border; solid black lines are the major faults separating the various terranes in SW Yunnan.

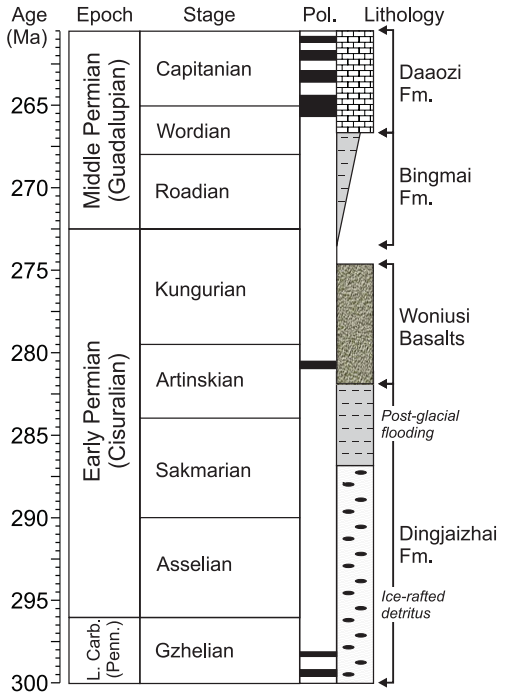

Figure 3. Summary of the Permian stratigraphy of the Baoshan block and relationship to wider-scale phenomena/features. The stage names follow Gradstein *et al.* (2005).

Baoshan has a distinctive late Palaeozoic geological sequence (Fig. 3; e.g. Wang *et al.* 2001; Jin 2002; Ueno 2003; Yan *et al.* 2004). The lower Dingjaizhai Formation contains ice-rafted detritus related to the glaciation that affected large parts of Gondwana; subsequent melting of the ice sheets saw the inundation of the continental margins due to raised global sea levels (upper Dingjaizhai Formation); the conodont assemblage *Sweetognathus whitei-Mesogondolella bisselli* is associated with this level, suggestive of a late Sakmarian-early Artinskian age (Ueno 2003). This was followed by an extensional phase that was accompanied by mafic volcanism (Woniusi Formation); conodonts extracted from intercalated limestones indicate a middle-late Artinskian to Kungurian age (Wang *et al.* 2004). The cessation of volcanism and initial drifting saw the accumulation of continental sediments (Bingma Formation), before shallow marine conditions returned with carbonate deposition (Daaozi Formation).

3 AN EARLIER PALAEOMAGNETIC INVESTIGATION

Two decades ago, Huang & Opdyke (1991) carried out a palaeomagnetic investigation of the Woniusi Basalts, reporting data from two localities close of Baoshan city, and a third from near Yongde town, ~120 km to the south. Their study can be regarded as 'modern' in that they sampled several cooling units in each of the three exposures; two of the outcrops are from opposing limbs of a large synform, thus the directional data could be subjected to a 'fold test'; detailed step-wise demagnetization was carried out, both alternating field and thermal; characteristic sample directions were calculated using principal component analysis. Huang & Opdyke's key finding was that the basalts had been erupted at ~42°S. Unfortunately, because of the overall lack of data that was then available for the broader region, discussions on the wider tectonic context were inevitably limited.

4 SAMPLING AND LABORATORY WORK

At each outcrop, a single oriented block, 500–700 cm^3, was collected from each of the cooling units (all bar one are flows, the other is a gabbroic dyke). Each individual cooling-unit block sample (ICUBS), therefore, represents a palaeomagnetic 'site' because the sample should provide an instantaneous record of the geomagnetic field a shortly after the magma had crystallized and the magnetic grains cooled below their blocking temperatures. There is, however, potential for blocks collected in this way to record small sampling-related orientation biases, which is not really a problem with field-based drill-cored collections. Therefore, we aimed to select reference surfaces with very different orientations to the others in the section. Furthermore, we collected as many cooling units as possible—one had 14. Another thing to note is that magnetic bearings were corrected to 'true' using the International Geomagnetic Field Model, version 11; at the time of sampling the offset was ~1°W.

In the University of Hong Kong laboratory, six to eight 2.54-cm-diameter by 2.15-cm-long drill core specimens were prepared from each block. Remanance measurements were carried out using an Agico JR6A spinner magnetometer. Both alternating field or/and thermal demagnetization were carried out on the individual specimens using, respectively, a Molspin alternating field tumbler system and a Magnetic Measurements' thermal demagnetizer. Characteristic magnetization directions were determined using principal component analysis (Kirschvink 1980) applied to data that had been plotted on vector-endpoint plots (Zijderveld 1967). In almost all cases, a stable single direction is observed above 10–20 mT/350–400 °C (Figs 4 and 5). However, the thermal demagnetization (Fig. 6, as well as Fig. 5) reveals that these directions are recorded either by magnetite (because they 'unblock' ≤578 °C, with a fairly sharp intensity decline just below this temperature) or magnetite plus variable fractions of haematite (which unblocks ≤680 °C) (N.B., the limited amount of demagnetization data presented by Huang & Opdyke (1991, figs 3 and 5) show similar features. To understand the phenomena, we compiled for each of the thermally processed specimens the ratio (per cent) of the remanance at 575 °C (J_{575}) relative to the initial value (J_{NRM}), listing in Table 1 the range of values for each block. In some cases, the numbers are rather low (e.g. WN3, WN12, WN23—see Fig. 6a), whereas in others they are notably higher (WN2, WN43, WN68—see Fig. 6b). From Table 1, there appears to be no stratigraphic control (e.g. Woniu Temple and Town 707 road-cut sections). Our favoured explanation is that the

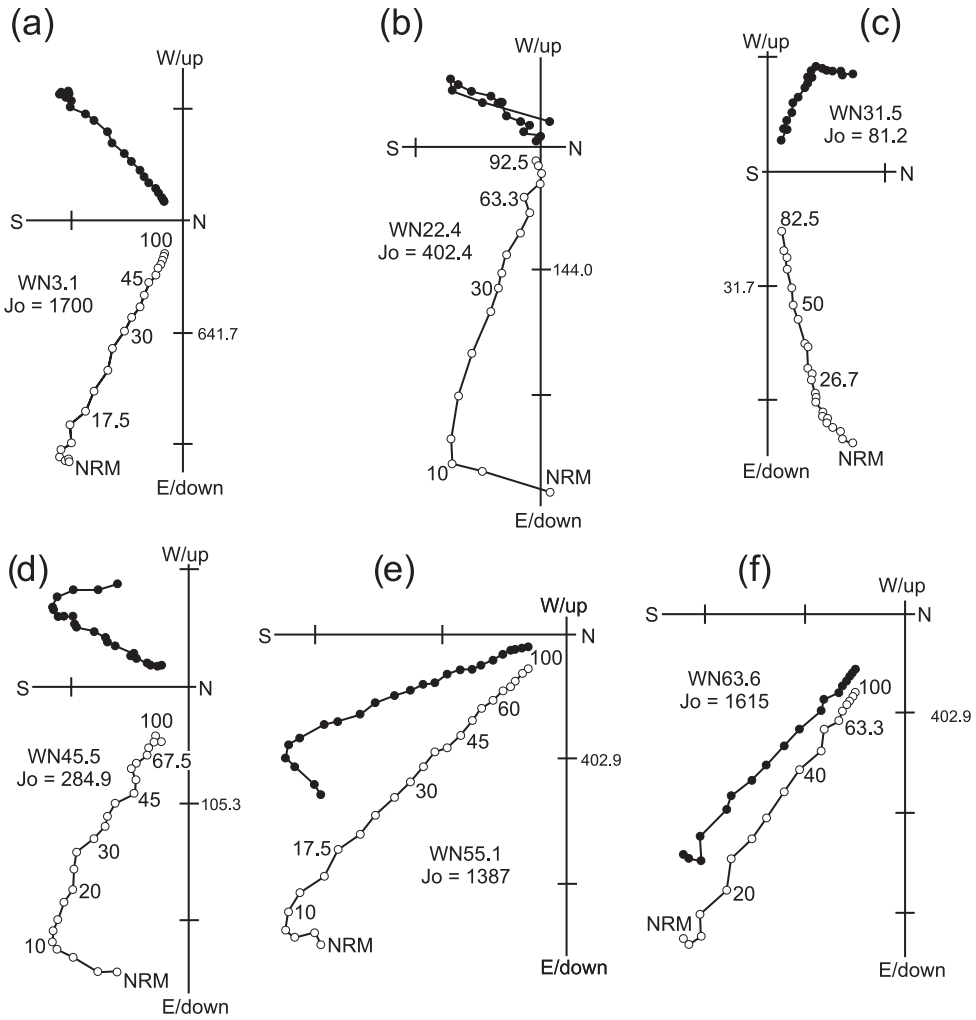

Figure 4. Examples of AF demagnetization data plotted on vector-endpoint plots (Zijderveld 1967). In all cases the data are shown in the tilt-corrected reference frame. Solid/open circles represent vectors projected onto the horizontal/vertical planes. For each sample, the identifier and initial natural remanent magnetization intensity (J_{NRM}) are shown (units being mA m^{-1}). Key demagnetization steps are also indicated (up to 100 mT) as well as scale bars on both axes.

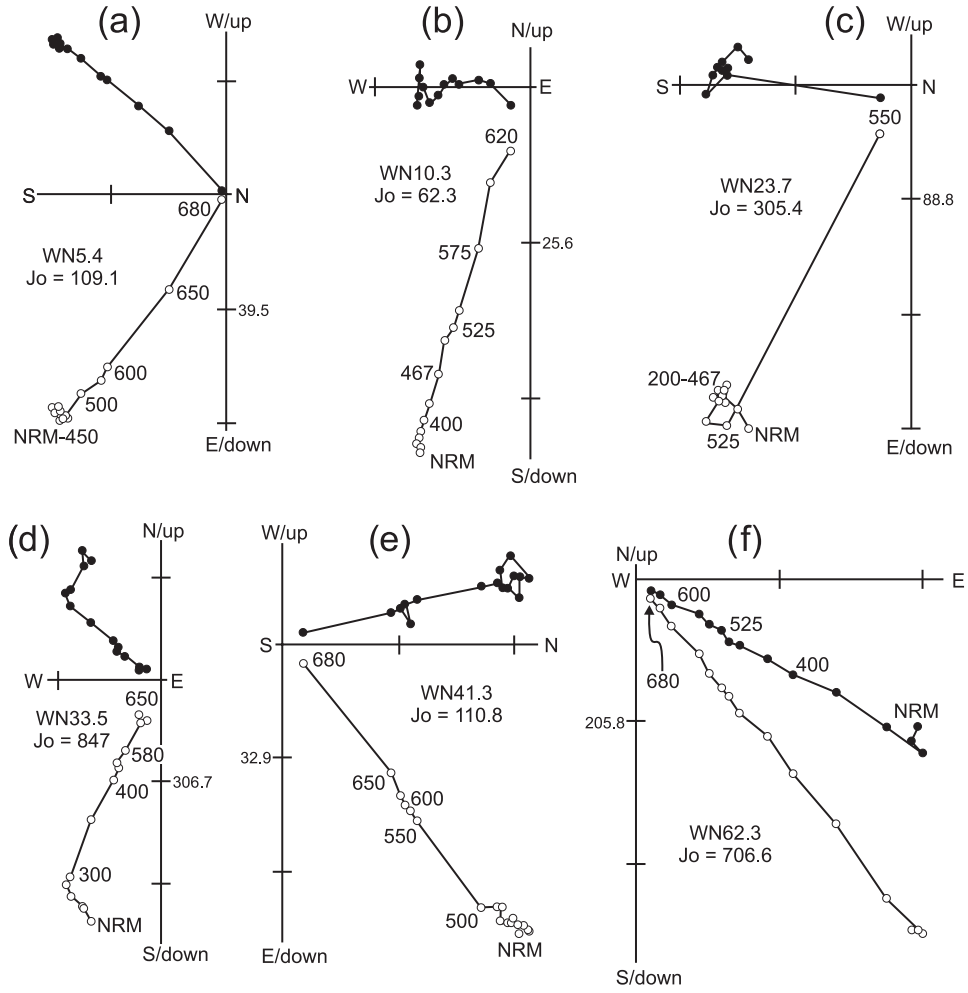

Figure 5. Examples of thermal demagnetization data plotted on vector-endpoint plots (Zijderveld 1967). In all cases the data are shown in the tilt-corrected reference frame. Solid/open circles represent vectors projected onto the horizontal/vertical planes. For each sample, the identifier and initial natural remanent magnetization intensity (J_{NRM}) are shown (units being mA m^{-1}). Key demagnetization steps (in °C) are also indicated as well as scale bars on both axes.

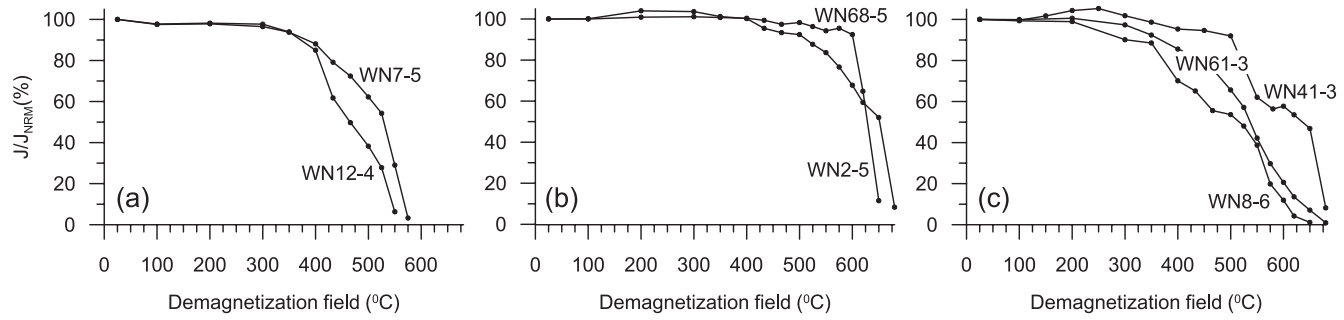

Figure 6. Representative thermal demagnetization decay plots revealing the principal magnetic minerals carrying the remanance: (a) magnetite dominates; (b) haematite dominates; (c) mixture of magnetite and haematite. J_{NRM} is the initial intensity, J is the intensity at specific demagnetization steps (°C). See also Table 1 and the text.

magnetite record is a primary signal, whereas the haematite component, where present, is an alteration remanance acquired shortly afterwards, very possibly before the next flow. Critically with this interpretation, if the high-coercivity magnetizations were even just several million years younger, with the volcanics erupting onto a rifting/northward drifting block, we would not anticipate them paralleling the low-temperature components.

Block-sample- and locality-mean directions were calculated using the statistics of Fisher (1953; see also Table 1).

5 RESULTS

5.1 Woniu Temple section, ENE of Baoshan City

14 separate cooling units, each 3–5 m thick, were sampled from the uppermost Woniusi Formation along what in March 2010 was a freshly excavated dirt track leading to the village of Daouzhi (Fig. 7; 25°09′ 06″ N, 099° 16′ 54″ E). The pathway runs behind and above the Woniu (not Woniusi) Temple, and is ∼12 km ENE of Baoshan

Table 1. Summary of the palaeomagnetic data from the newly studied sections reported in this study. ICUBS, individual cooling unit block sample; Nc(Np), number of specimens from a site used to calculate the mean direction from the number of specimens processed; Nt, number of specimens/block sample that were processed exclusively by thermal demagnetization or a combination of AF followed by thermal demagnetization. The column J_{575}/J_{NRM} records for each block the specimen with the minimum and maximum values of the ratio (as per cent) of the intensity at 575 °C/initial value. See also Fig. 6. Abbreviations α_{95} and ∗AS, respectively, indicate the 95 per cent confidence circle radius and the angular separation between two directions.

ICUBS	Strike/Dip/DD	Nc(Np)Nt	Range of J_{575}/J_{NRM} per cent	*In situ* Dec	*In situ* Inc	Tilt corrected Dec	Tilt corrected Inc	α_{95}/ ∗AS	k	Used in loc. mean calc.
Boashan area: Woniu Temple (25° 09′ 06″ N, 099° 16′ 54″ E)										
WN1	000/12/ESE	6(6)4	8–18	222.7	39.8	213.7	47.3	4.4	233.0	Y
WN2	000/12/ESE	6(6)4	93–95	225.3	42.4	215.8	50.2	1.9	1284.5	Y
WN3	000/12/ESE	6(6)2	10–10	236.8	43.2	228.7	52.9	3.2	426.0	Y
WN4	000/12/ESE	6(6)4	30–32	223.9	30.6	217.6	38.4	1.8	1366.3	Y
WN5	000/12/ESE	6(6)4	55–76	228.2	33.9	221.5	42.4	4.8	195.0	Y
WN6	000/12/ESE	6(6)2	12–15	256.3	54.7	250.1	66.2	2.9	543.1	Y
WN7	340/15/ENE	7(7)1	3	263.3	59.7	261.6	63.4	2.7	494.0	Y
WN8	340/15/ENE	6(6)4	16–20	264.1	53.8	267.3	68.7	1.6	1822.7	Y
WN9	340/15/ENE	7(7)1	40	257.9	48.6	274.8	74.0	4.1	218.0	Y
WN10	340/15/ENE	6(6)2	42–44	258.6	56.6	264.9	71.3	1.3	2645.6	Y
WN11	340/15/ENE	7(7)3	12–12	262.9	59.0	273.6	73.3	1.0	3451.0	Y
WN12	340/15/ENE	6(6)3	2–10	255.0	46.4	257.2	61.3	1.7	1565.2	Y
WN13	340/15/ENE	6(6)0	NA	249.8	43.9	249.7	58.9	8.2	68.4	Y
WN14	346/12/ENE	6(6)0	NA	247.4	63.8	240.7	75.6	2.5	728.6	Y
	Mean IS	14(14)		244.4	49.4	—	—	7.3	30.9	
	Mean TC	14(14)		—	—	238.8	62.0	8.1	24.9	
Boashan area: Guanpo Village area (25° 12′ 36′N, 099° 15′ 41″ E)										
WN21	027/26/ESE	8(8)2	28–33	246.9	55.2	203.0	64.0	3.8	213.6	Y
WN22	027/26/ESE	6(6)0	NA	261.5	64.8	188.0	74.8	7.1	90.9	Y
WN23	027/26/ESE	8(8)2	2–2	230.7	56.3	189.1	57.7	6.8	67.8	Y
	Mean	3(3)		245.1	59.3	193.8	65.6	14.3	75.9	
Boashan area: Small hydroelectric dam NW of Guanpo Village (25° 13′ 30″ N, 099° 16′ 55″ E)										
WN31	032/15/SE	6(6)0	NA	300.2	49.9	299.4	64.9	3.1	476.0	Y
WN33	032/15/SE	6(6)4	18–30	309.4	45.4	312.5	60.3	4.3	239.8	Y
WN35	032/15/SE	5(6)0	NA	309.2	66.8	321.5	81.5	4.1	356.3	Y
WN36	032/15/SE	6(6)2	20–22	224.4	64.3	193.3	63.4	4.5	224.4	No
	Mean	3(4)		306.0	54.1	308.5	69.1	17.9	48.2	
Boashan area: 3 km SW of Haitangwa Village (25° 15′ 03″ N, 099° 18′ 09″ E)										
WN41	230/14/NW	6(6)4	56–61	57.0	70.8	19.8	67.8	4.4	234.1	Y
WN43	230/14/NW	6(6)3	68–89	290.8	45.7	295.9	33.1	1.1	3589.6	Y
WN44	230/14/NW	6(6)4	34–55	166.8	60.0	185.3	71.5	3.1	458.4	Y
WN45	230/14/NW	6(6)4	26–41	189.8	53.7	208.7	60.9	7.5	87.4	Y
WN47	230/14/NW	8(8)2	20–32	249.9	80.9	293.0	70.9	9.8	32.7	Y
	Mean	5(5)		216.3	78.7	275.1	74.3	31.8	6.7	
Town 707 area: Suanpashan quarry (24° 53′ 41″ N, 099° 07′ 10″ E)										
WN53	305/29/NE	6(6)0	NA	185.0	33.1	166.4	56.0	3.4	386.9	Y
WN55	305/29/NE	6(6)0	NA	173.0	21.2	159.6	40.7	3.0	501.0	Y
	Mean	2(5)		178.7	27.3	162.5	48.4	∗15.9	NA	
Town 707 area: Road cutting ∼2 km from Town 707 (24° 54′ 59″ N, 099° 05′ 09″ E)										
WN61	295/76/NNE	8(8)4	24–46	161.5	−5.8	136.8	42.5	2.8	379.9	Y
WN62	295/76/NNE	6(6)4	13–19	162.2	8.7	117.5	47.7	5.3	159.3	Y
WN63	295/76/NNE	6(6)2	20–21	165.3	6.7	121.4	50.3	3.8	309.3	Y
WN64	295/76/NNE	6(6)4	37–68	158.8	3.6	123.4	43.3	3.8	306.4	Y
WN65	295/76/NNE	8(8)4	15–25	155.4	−3.2	130.5	37.9	1.1	2456.5	Y
WN66	295/76/NNE	6(6)4	56–66	149.5	3.8	120.0	34.3	1.1	3891.6	Y
WN67	295/76/NNE	7(7)3	48–63	168.7	7.7	121.2	53.8	2.2	765.9	Y
WN68	295/76/NNE	8(8)3	67–77	165.9	5.2	123.9	50.6	5.1	173.0	Y
	Mean	8(8)		160.9	3.4	124.5	45.2	5.6	99.8	

City. The sequence dips in an easterly direction at 12–15°, the strike being due north in the upper part of the section and ∼340° in the lower part. Useful data were obtained from each of the flows: the *in situ* mean direction is Dec = 244.4°, Inc = 49.4°, α_{95} = 7.3° and k = 30.9, whereas the tilt-corrected mean direction is Dec = 240.0°, Inc = 60.7°, α_{95} = 8.1°, k = 24.9 (Table 1, Fig. 8).

5.2 Near Guanpo Village, NE of Baoshan City

Samples from three cooling units were collected along cuttings flanking the unsealed road leading to the mine near Guanpo, about 14 km ENE of Baoshan City (Fig. 7; 25° 12′ 36′ N, 099° 15′ 41″ E). Two eruptive horizons exhibiting pepperite textures (WN21–22)

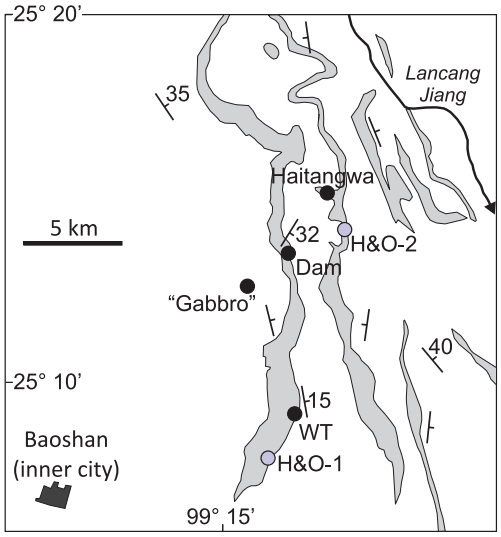

Figure 7. Simplified geological map showing the Woniusi Formation (grey) sampling localities to the east and northeast of Baoshan City.

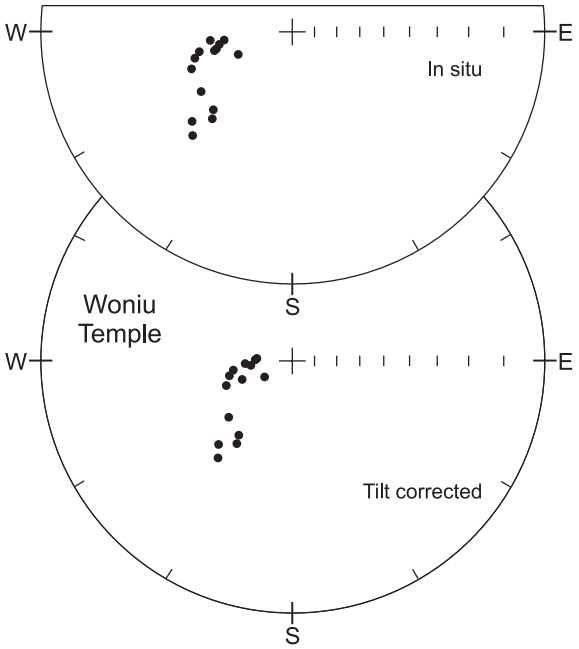

Figure 8. Equal-angle stereonet plots of *in situ* (top) and tilt-corrected (bottom) site mean data from the section close to Woniu Temple (also see Table 1). All directions are downward dipping. The α_{95} values are listed in Table 1; range 1.0–8.2°.

were collected, together with one sample (WN23) from an immediately adjacent gabbroic dyke (>100 m wide). The sequence dips 26° towards the ESE. The *in situ* mean direction is Dec = 245.1°, Inc = 59.3°, α_{95} = 14.3° and k = 75.7; the tilt-corrected mean direction is Dec = 193.8°, Inc = 65.6°, α_{95} = 14.3° and k = 75.9 (Table 1, Fig. 9).

5.3 Small hydroelectric dam near Guanpo Village, NE of Baoshan City

Five cooling units were sampled (WN31–5) just below a small hydroelectric dam (Fig. 7; 25° 13′ 30″ N, 099° 16′ 55″ E) close to the village of Guanpo, ~17 km northeast of Baoshan City. The exposure

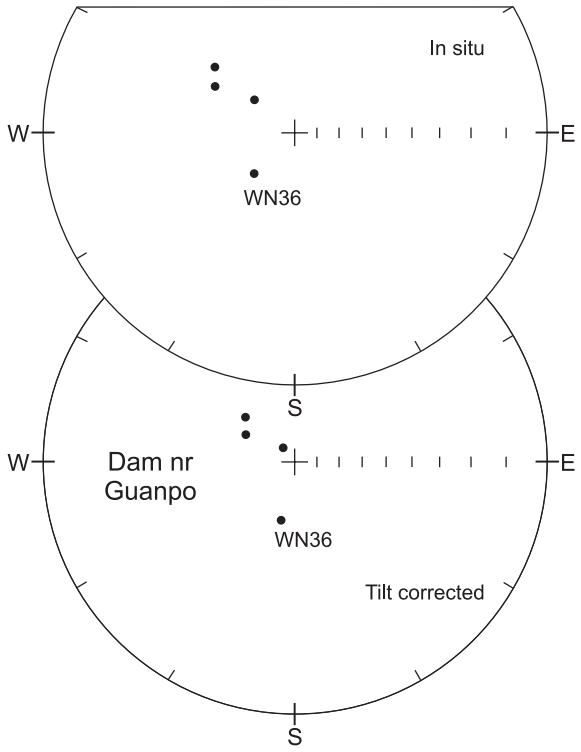

Figure 9. Equal-angle stereonet plots of *in situ* (top) and tilt-corrected (bottom) site mean data from the dirt track near Guanpo Village (also see Table 1). All directions are downward dipping. The α_{95} values are listed in Table 1; range 3.8–6.8°.

contains several 3- to 5-m-thick basalt flows that dip 15° towards the southeast. A fine-grained 4-m-thick limestone is present in the sequence (between samples WN34 and WN35), indicating that the eruptions spanned, from a palaeomagnetic perspective, a reasonable period of time. Above the valley, ~100 m from the dam, a sixth block (WN36), was collected from the floor of the old trail that parallels the road. Although four blocks yield meaningful directional data, the locality mean has been calculated without WN36 due to it sitting some distance from the main cluster (Table 1, Fig. 10). The *in situ* direction is Dec = 306.0°, Inc = 54.1°, α_{95} = 17.9° and k = 48.2; after tilt correction, this corresponds to Dec = 308.5°, Inc = 69.1° (inclusion of WN36, results in Dec = 283.5°, Inc = 75.3°, but α_{95} = 25.8° and k = 13.7).

5.4 Close to Haitangwa Village, NE of Baoshan City

Further along the road from Guanpo Village, about 3 km before Haitangwa Village, a slightly overgrown road cutting exposes the uppermost Woniusi Basalts and the basal Daaozi Formation (Fig. 7; 25° 15′ 03″ N, 099° 18′ 09″ E). Seven blocks were sampled (WN41–7) from individual flows that stratigraphically span 35–40 m (dip is ~14° to the northwest). Although five sites yielded meaningful data, the mean direction in both *in situ* and tilt-corrected coordinates is too scattered (Table 1, Fig. 11; α_{95} = 31.8°, k = 6.7) to be used for tectonic modelling.

5.6 Two Baoshan area outcrop results reported by Huang & Opdyke (1991)

As mentioned, Huang & Opdyke (1991) reported data from two Woniusi Basalt sections close to Baoshan City. At the first of these,

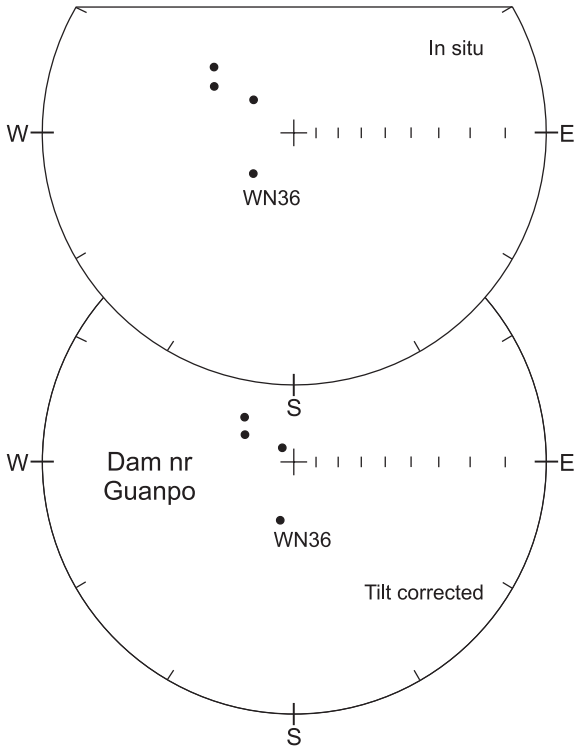

Figure 10. Equal-angle stereonet plots of *in situ* (top) and tilt-corrected (bottom) site mean data from the hydroelectric dam section near Guanpo (also see Table 1). All directions are downward dipping. The α_{95} values are listed in Table 1; range 3.1–4.5°.

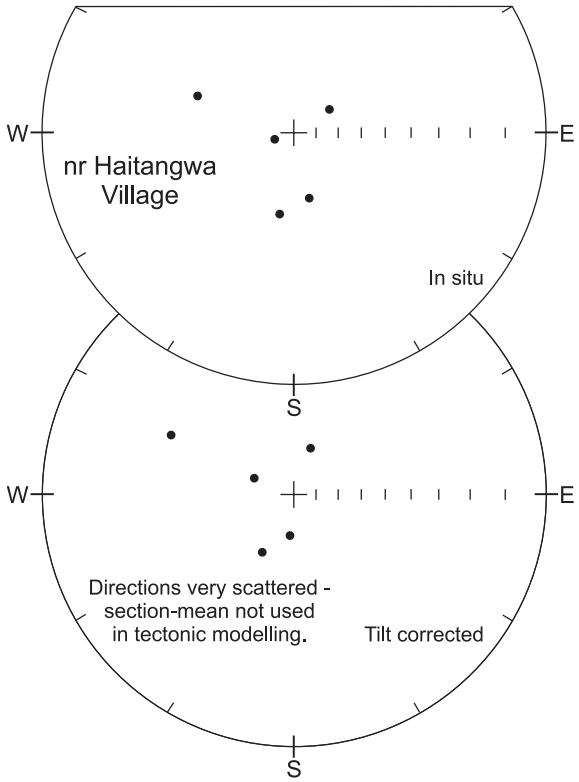

Figure 11. Equal-angle stereonet plots of *in situ* (top) and tilt-corrected (bottom) site mean data from the section close to Haitangwa Village (also see Table 1). All directions are downward dipping. The α_{95} values are listed in Table 1; range 1.1–9.8°.

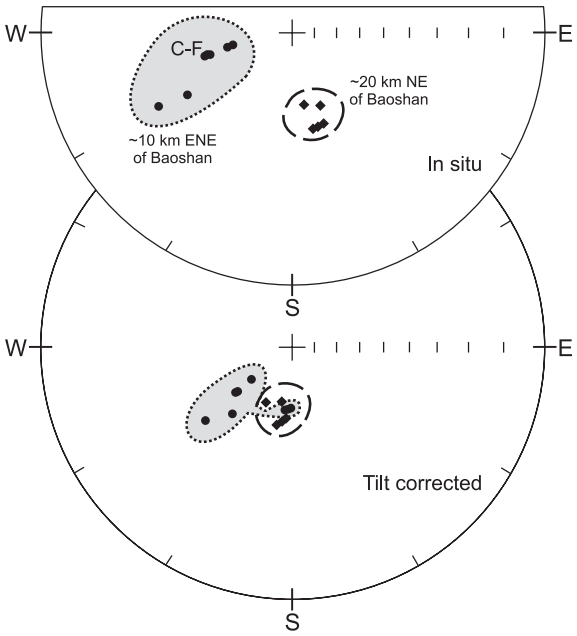

Figure 12. Equal-angle stereonet plots of *in situ* (top) and tilt-corrected (bottom) site mean data from the two sections studied by Huang & Opdyke (1991) close to Baoshan City. All directions are downward dipping: circles are for the section ~12 km ENE of the city ('25.2°N, 99.3°E'); diamonds are for the section ~19 km to the northeast of Baoshan (see Fig. 2). The α_{95} values are listed in Table 2; range 2.0–8.9°.

eight sites (labelled A–H) from an exposure 10 km ENE of the city (Fig. 7) yielded useful directions. The *in situ* mean direction is Dec = 250.9°, Inc = 49.7°, α_{95} = 8.7° and k = 41.6, whereas the tilt-corrected mean direction is Dec = 220.1°, Inc = 60.2°, α_{95} = 9.3° and k = 60.2 (Fig. 12, Table 2). At the second exposure, ~20 km northeast of the city, five sites (I–M) recorded directions that could be used in plate modelling: the *in situ* mean is Dec = 164.5°, Inc = 51.7° whereas the tilt-corrected mean is Dec = 192.0°, Inc = 62.4° (α_{95} = 5.4° and k = 203.6; Fig. 12, Table 2).

5.7 Suanpashan Quarry Area, Youwang Town

The Suanpashan quarry section is ~5.5 km southeast of the unusually named 'Town 707' (Fig. 13, 24° 53′ 41″ N, 099° 07′ 10″ E; it is 25–30 km south of Baoshan City). Five sites (WN51–55) were collected from a semi-continuous exposure of the upper Woniusi Formation next to an unsealed road that leads to an excavation where Daaozi Formation limestones are being extracted. Two of the sites (WN53, WN55) yielded directional data (Fig. 14, Table 1): the *in situ* mean is Dec = 178.7°, Inc = 27.3°, whereas the tilt-corrected Dec = 162.5°, Inc = 48.4°, where the angular separation (not Fisher mean) is 15.9°. Unfortunately, the limited size of the data set obtained for this section means that we exclude it from our formation-mean calculation—see later.

5.8 Temporary road cutting southeast of Town 707

During sampling in March 2010, it was possible to access a Woniusi Formation sequence exposed in an under-construction road-cutting 1.3 km southeast of Town 707 (Fig. 13, 24° 54′ 59″ N, 099° 05′ 09″ E). There, the approximately 30-m-thick sequence of thin volcanic

Table 2. Summary of the palaeomagnetic data from the sections studied by Huang & Opdyke (1991). Nc(Np), number of specimens from a site used to calculate the mean direction from the number of specimens processed.

		In Situ		Tilt corrected				Used in loc.
Site	Strike/Dip/DD	Dec	Inc	Dec	Inc	α_{95}	k	mean calc.
Baoshan-1								
A	014/21/ESE	239.4	38.4	222.4	51.2	6.7	130.5	Y
B	014/21/ESE	241.1	27.6	230.2	41.7	6.1	156.3	Y
C	014/21/ESE	255.4	50.7	232.6	67.2	2.0	1397.9	Y
D	014/21/ESE	255.3	50.4	232.6	66.9	4.9	241.4	Y
E	042/17/SE	255.1	52.8	231.3	59.1	2.6	886.8	Y
F	042/17/SE	255.2	51.9	232.1	58.3	8.9	74.8	Y
G	040/35/SE	257.7	60.6	186.7	62.3	8.6	81.0	Y
H	040/35/SE	258.5	63.0	181.8	63.1	4.7	266.5	Y
Mean IS (8/8)		250.9	49.7	—	—	8.7	41.6	
Mean TC (8/8)		—	—	220.1	60.2	9.3	36.2	
Baoshan-2								
I	203/20/WNW	167.8	47.6	191.4	55.7	4.9	240.6	Y
J	203/20/WNW	170.6	57.9	205.9	63.3	4.1	503.6	Y
K	203/20/WNW	158.7	55.8	191.0	65.7	2.3	824.5	Y
L	203/20/WNW	164.5	47.9	188.2	57.2	6.9	124.0	Y
M	203/20/WNW	161.1	48.7	185.3	59.0	2.8	751.0	Y
Mean (5/5)		164.5	51.7	192.0	60.4	5.4	203.6	
Yongde								
N	022/37/ESE	286.1	23.0	281.1	59.7	3.1	618.6	Y
O	022/37/ESE	283.0	19.5	276.7	55.7	3.0	635.1	Y
P	022/37/ESE	306.7	27.7	320.5	62.5	5.7	181.8	Y
Q	022/37/ESE	301.2	27.4	310.6	63.5	4.4	275.7	Y
R	022/37/ESE	290.7	33.4	288.9	70.4	4.5	294.2	Y
S	022/37/ESE	292.9	29.2	293.9	66.2	2.3	1147.0	Y
T	010/40/E	289.5	56.3	61.7	81.5	13.6	25.3	No
U	010/40/E	313.9	71.2	75.9	63.7	14.6	28.3	No
Mean (6/8)		293.3	26.9	294.5	63.9	7.8	74.2	

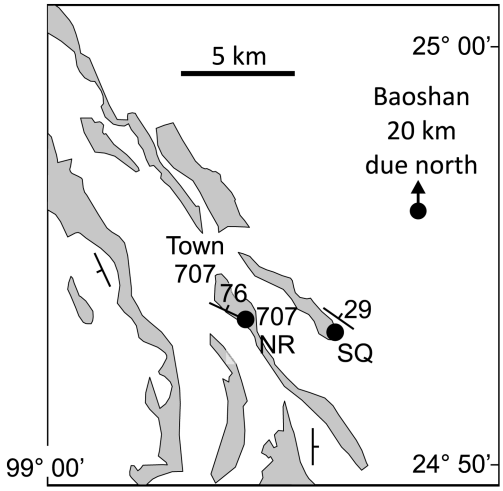

Figure 13. Simplified geological map showing the Woniusi Formation (grey) sampling localities close to Town 707.

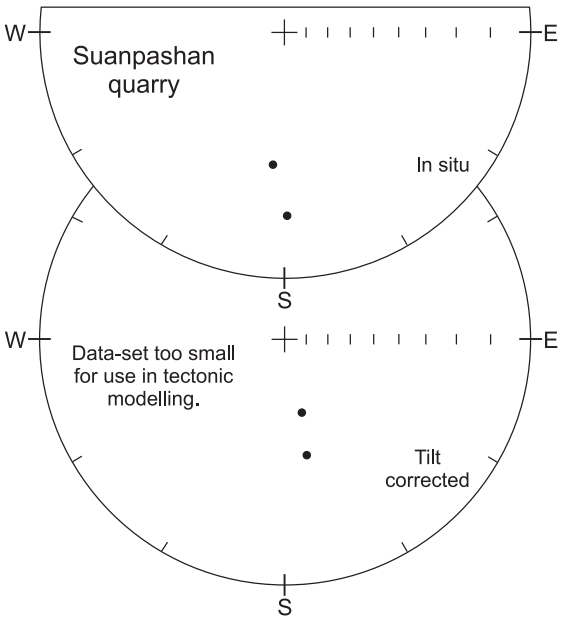

Figure 14. Equal-angle stereonet plots of *in situ* (top) and tilt-corrected (bottom) site mean data from the section close to and stratigraphically below the limestone quarry at Suanpashan (also see Table 1). Both directions are downward dipping. The α_{95} values are listed in Table 1; range 3.0–3.4°.

and sedimentary horizons dips 76° to the NNE. All eight cooling units that were sampled yielded useful data; the *in situ* mean is Dec = 160.9°, Inc = 3.4°; after tilt correction, Dec = 124.5°, Inc = 45.2° (α_{95} = 5.6° and k = 99.8; Table 1 and Fig. 15).

5.9 Results reported by Huang & Opdyke (1991) from a section near Yongde

Huang & Opdyke (1991) presented data from a Woniusi Basalt section near Yongde, ~120 km south of Baoshan City. Although they reported data from eight sites (N–U), they calculated a locality mean using directions from just six (N–S; see Huang & Opdyke 1991, pp. 339–340). The *in situ* Dec = 293.3°, Inc = 26.9°, whereas the tilt-corrected value is Dec = 294.5°, Inc = 63.9° (α_{95} = 7.8° and k = 74.2; Table 2 and Fig. 16).

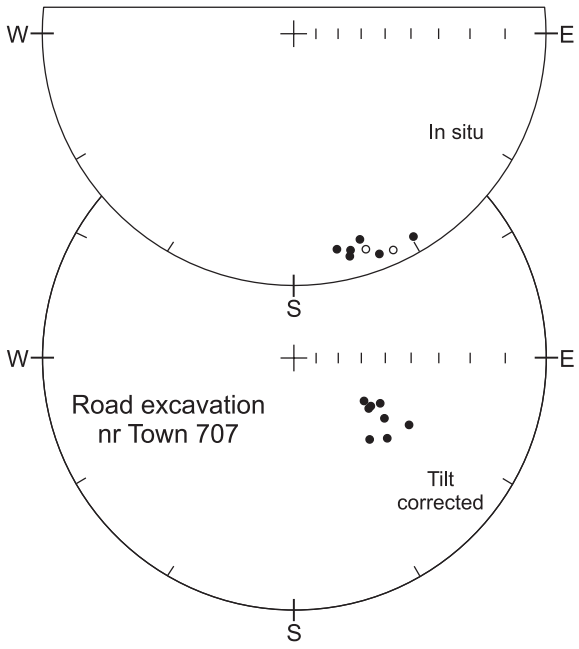

Figure 15. Equal-angle stereonet plots of *in situ* (top) and tilt-corrected (bottom) site mean data from the 2010 road-cutting excavation ~2 km southeast of Town 707 (also see Table 1). Solid/open circles represent downward-/upward-dipping directions. The α_{95} values are listed in Table 1; range 1.1–5.3°.

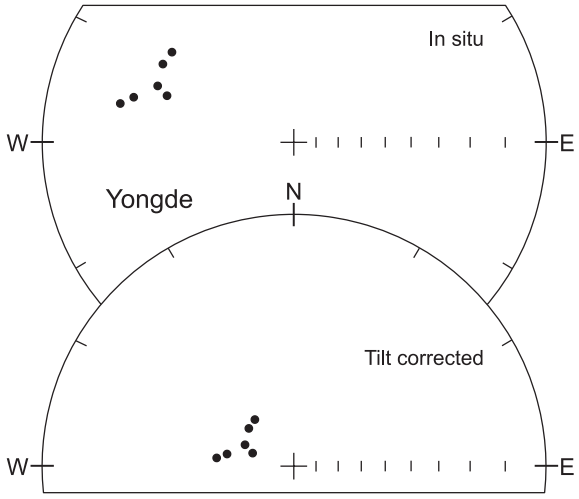

Figure 16. Equal-angle stereonet plots of *in situ* (top) and tilt-corrected (bottom) site mean direction data from the section studied by Huang & Opdyke (1991) close to Yongde City ('23.9°N, 99.2°E'). The α_{95} values are listed in Table 2; range 2.3–5.7°.

6 SUMMARY OF THE MAGNETIZATION DIRECTIONS

Combining the new palaeomagnetic results with those of Huang & Opdyke (1991) means that the Woniusi Formation data set is now based on directions from seven localities/47 cooling units. As can be seen from Fig. 17, in tilt-corrected coordinates each locality direction is moderately steep and downward dipping, which correspond to reverse polarity magnetizations acquired at mid-Southern Hemisphere latitudes. The absence of any normal polarity sites is explained by the fact that the volcanic rocks were erupted in the mid-Early Permian, ~280 Ma, two-thirds through the Kiaman Reverse Polarity Superchron (311.7–265.8 Ma; Gradstein *et al.* 2005). An-

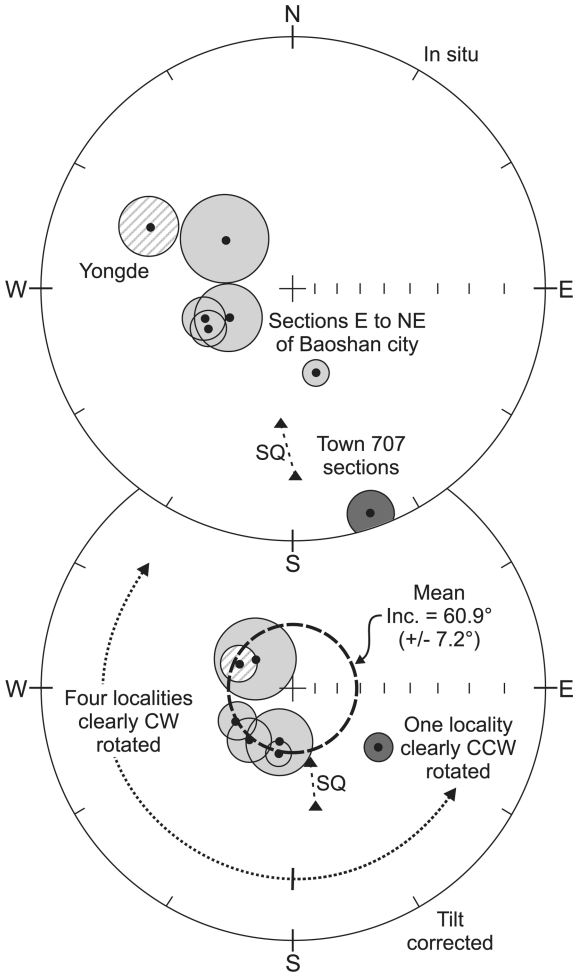

Figure 17. Summary of all screened locality mean data (top: *in situ*; bottom: tilt-corrected). Small solid/open circles represent downward-/upward-dipping directions, larger circles are the 95 per cent confidence ellipses. Thick dashed line centred on the vertical is the mean inclination angle. The directions from the basalt exposures near the limestone quarry Suanpashan (SQ) are also shown (black triangles), but they are excluded from the formation-mean calculation.

other feature is that the declinations indicate that the exposures have each experienced variable vertical-axis rotations, principally clockwise, but sometimes counterclockwise. It must be noted, though, that these offsets almost certainly include a significant clockwise component (30–40°) that has been induced by the Indian block's indentation into Asia in the middle and late Cenozoic (see Socquet & Pubellier 2005; Otofuji *et al.* 2010; Yamashita *et al.* 2011; Kondo *et al.* 2012). Consequently, the formation-mean inclination is calculated using the statistics of McFadden & Reid (1982; rather than Fisher 1953): Inc = 60.9°, where $\alpha_{95} = 7.2°$ and $k = 55.6$ (Table 3). This compares favourably with the *in situ* value where the associated scatter is much larger (Inc = 42.5°, $\alpha_{95} = 19.1°$, $k = 8.4$) suggesting that the remanance is pre-tilting, probably primary. The resulting formation latitude is 41.9°S; with errors, the permissible range is 34.2°S–51.2°S. It is also worth noting that the directions from the five sections to the east and northeast of Baoshan City (Fig. 7), show a tighter clustering after the tilt corrections have been applied ($\alpha_{95} = 17.6°$, $k = 20.0$) as compared with their equivalents in the geographic reference frame ($\alpha_{95} = 27.5°$, $k = 8.7$). As the studied outcrops are from different parts of a large synform, it strongly suggests that the magnetizations pre-date the folding.

Table 3. Summary of the outcrop-level palaeomagnetic data (based on data in Tables 1 and 2). Nc(Np), number of specimens from a site used to calculate the mean direction from the number of specimens processed. McFadden & Reid (1982) is abbreviated to M&R. Abbreviations α_{95} and *AS, respectively, indicate the 95 per cent confidence circle radius and the angular separation between two directions.

Location	Nc(Np)	*In situ* Dec	*In situ* Inc	Tilt corrected Dec	Tilt corrected Inc	α_{95}/ *AS	k	Used in form. mean calc.
Woniusi Temple IS	14(14)	244.4	49.4	—	—	7.3	30.9	Y
Woniusi Temple TC	14(14)	—	—	238.8	62.0	8.8	21.6	Y
Gabbro	3(3)	245.1	59.3	193.8	65.6	14.3	75.9	Y
Hydro dam	3(4)	306.0	54.1	308.5	69.1	17.9	48.2	Y
Near Haitangwa	5(5)	216.3	78.7	275.1	74.3	31.8	6.7	No
H&O-Baoshan-1 IS	8(8)	250.9	49.7	—	—	8.7	41.6	Y
H&O-Baoshan-1 TC	8(8)	—	—	220.1	60.2	9.3	36.2	Y
H&O-Baoshan-2	5(5)	164.5	51.7	192.0	60.4	5.4	203.6	Y
Town 707-Suanpashan quarry	2(5)	178.7	27.3	162.5	48.4	*15.9	NA	No
Town 707-Road	8(8)	160.9	3.4	124.5	45.2	5.6	99.8	Y
H&O-Yongde	6(8)	293.3	26.9	294.5	63.9	7.8	74.2	Y
Mean M&R IS	7(9)	—	42.5	—	—	19.1	8.4	
Mean M&R TC	7(9)	—	—	—	60.9	7.2	55.6	

7 IMPLICATIONS FOR TECTONIC MODELLING

7.1 Positioning Baoshan against Gondwana

Based on the newly acquired palaeolatitudinal data, Fig. 18 shows how Baoshan likely once sat adjacent to Gondwana. The stencil for the supercontinent is from the library associated with the GMAP software (Torsvik & Smethurst 1999); it has been rotated into its Early Permian (280 Ma) position using data from Torsvik *et al.* (2008). Greater India is based on Ali & Aitchison (2005)—see also Colwell *et al.* (1994) and Stilwell *et al.* (2012) concerning the basement forming the Wallaby and Zenith plateaus. The suggestions of Hall (2011) underpin the modelling of the small blocks immediately northwest of Australia, as well as the Sula Spur to the west of New Guinea. Palaeomagnetic data from northern Iran (Wensink 1979; Besse *et al.* 1998; predicted palaeo-latitude is 13°±) are used to position the Alborz block against northern Arabia. Together, the options for fitting Baoshan against the supercontinent are ostensibly limited to the small region where margins of northern Greater India and northwestern Australia once met. In this reconstruction it is at ~73°E, but potentially between 65° and 85° east if the palaeolatitudinal error-range is considered.

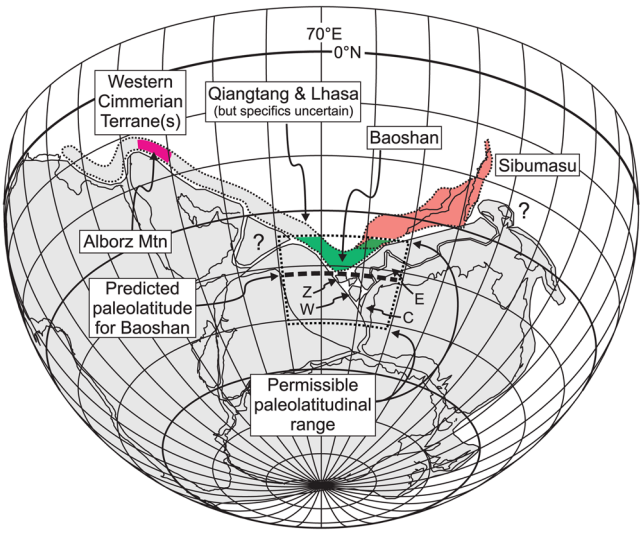

Figure 18. Placing Baoshan alongside eastern Gondwana in the mid-Early Permian (280 Ma; modelling done using the GMAP software of Torsvik & Smethurst 1999). The supercontinent is positioned using information in Torsvik *et al.* (2008, table 6, 'Global Hybrid' column). Note that Sibumasu (east of the modelled position for Baoshan) and northern Australia were not directly adjacent and were separated by crustal blocks that rifted from the latter in the Middle to Late Jurassic (see text). Abbreviations: C, E, W and Z, respectively refer to the Carnarvon Terrace and Exmouth, Wallaby and Zenith plateaus that sit W and NW of Australia. Regarding the latter three, they have been 'nudged' in a southeasterly direction to accommodate extension associated with the Late Jurassic–Early Cretaceous rifting that affected the wide region.

7.2 Implications for positioning the other eastern Cimmeria blocks

With Baoshan 'fixed' relatively tightly, it is possible to consider the wider geotectonic implications. First, however, it is necessary to summarize the various proposals that have linked the block to the other eastern Cimmerian terranes, specifically Qiangtang, Lhasa and Sibumasu. In all cases, correlations have been based on their present-day positions and structural relationships combined with the stratigraphic records. A sizeable majority of researchers consider Baoshan to be the northern tip of Sibumasu (Burrett *et al.* 1990; Nie *et al.* 1990; Huang & Opdyke 1991; Yan & Yin 2000; Yan & Zhao 2001; Shi 2003; Ueno 2003; Jian *et al.* 2009; Muttoni *et al.* 2009). A smaller number place it at the eastern end of Lhasa (Wang *et al.* 1996; Wopfner 1996; Jin 2002; Wopfner & Jin 2009). Others propose that it sat at the boundary between the conjoined Qiangtang–Sibumasu blocks (Metcalfe 1996, 2011; Li *et al.* 2004). Veevers & Tewari (1995) and Ferrari *et al.* (2008) prefer the Lhasa–Sibumasu junction.

Thus with an Early Permian reconstruction, it would seem logical to position Sibumasu east of Baoshan and to run the terrane (which is today ~4000 km long) along NW Australia (Fig. 18). However, we emphasize the fact that it must be some distance out from the present-day coast to accommodate the wide shelf, plus the fact that a number of terranes now in SE Asia rifted from the margin in the Middle to Late Jurassic (Hall 2011; Metcalfe 2011). Lhasa and Qiangtang almost certainly lay to the west, but the limited available information makes it difficult to propose their exact configuration. For instance, Metcalfe (2011) has argued that the two blocks were 'stacked' against Greater India, but they could have been

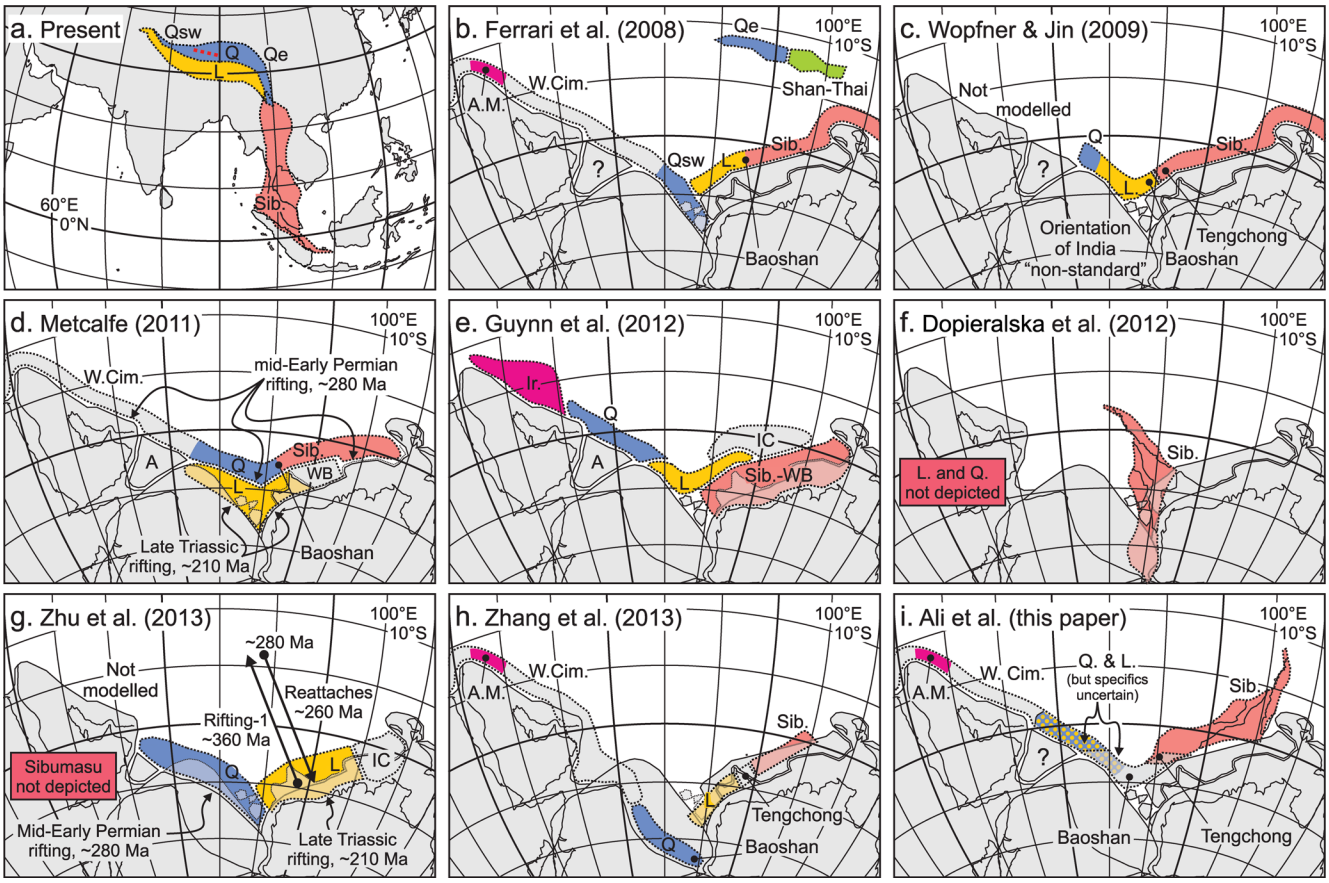

Figure 19. Summary of a number of recently proposed site-of-origin models for the Cimmerian terrane blocks. As a scale guide, the top left-hand panel (a) shows the various terranes in their present-day positions; latitude/longitude lines have 10° spacings, with the ones at 30°, 60°, etc. emphasized. For ease of comparison, all reconstructions use the 280 Ma Gondwana template adopted in Fig. 18. Abbreviations: A, Afghanistan; A.M., Alborz Mountains; IC, Indochina; Ir., Iran; L, Lhasa; Q, Qiangtang; Qsw, Southwest Qiangtang; Qe, eastern Qiangtang; Sib., Sibumasu; WB, West Burma (in some earlier works, "Mount Victoria Land"); W. Cim., Western Cimmeria.

along-strike from one another, or even had an overlapping layout (see next section). Finally in this section, we note that our model shows many similarities to one proposed over three decades ago by Şengör *et al.* (1980, fig. 1).

7.3 Comparison with recent model proposals

Despite four decades of deliberation (e.g. Ridd 1971; Audley-Charles 1983; Burrett *et al.* 1991), current opinion regarding the pre-rift locations of Sibumasu, Lhasa and Qiangtang remains widely divided (Fig. 19). For instance, Ferrari *et al.* (2008, fig. 9) split Qiangtang into an eastern and a southwestern block. The former was placed against northern India, and Lhasa and Sibumasu some distance out from the present-day northwest Australia–northern New Guinea continental shelf (Fig. 19b). Southwest Qiangtang is problematic in that the southeast portion would have overlapped the Wallaby and Zenith Plateaus; Lhasa is a little too short (*cf.* Fig. 19a). Notably, though, Baoshan is depicted and although it is some distance east of our suggested location, it is within the lower latitudinal error limit imposed by the palaeomagnetic data. Furthermore, the inferred position for the Iranian block is compatible with the Alborz Mountain palaeomagnetic data set (Wensink 1979; Besse *et al.* 1998).

Allowing for the non-standard positioning of India against eastern Antarctica–western Australia (*cf.* the classic 'tight-fit' reconstruction of Smith & Hallam 1970), Wopfner & Jin (2009, fig. 1), as well as Wopfner (1996) and Jin (2002), placed Lhasa and Qiangtang (based on the Orba Lake section towards the western end of the terrane) along-strike from one another off northern India, the former to the west; Sibumasu extends along northwest Australia (Fig. 19c). They also depicted the Baoshan and Tengchong blocks, the pair sitting, respectively, at the eastern and western ends of Lhasa and Sibumasu. Their positioning of Baoshan is compatible with the new palaeolatitudinal information.

Metcalfe (2011, fig. 15) retains his long-held view (e.g. Metcalfe 1996, 1998, etc): Sibumasu off NW Australia, Qiangtang and then Lhasa off India (Fig. 19d). A flaw with this model is block onlap, with Lhasa running over northern Greater India, as well as the Wallaby, Zenith and Exmouth plateaus. Setting aside this problem, Sibumasu and Qiangtang rifted-off as a conjoined ribbon in the Early Permian; Lhasa departed ~70 Myr afterwards in the Late Triassic. The Woniusi Basalt magnetizations would fit this model. Unfortunately, Metcalfe has never specified in detail how the various western Cimmerian subblocks abutted the NW India–NE Arabia portion of Gondwana, so we do not know where he might fit the Alborz block into the puzzle.

Shi *et al.* (2011) did not produce a tectonic model, but based on the fusulinid content of the Dingjiazhai Formation that lies directly beneath the Woniusi Basalts, they suggested Baoshan that during the Early Permian was close to the East-Central Iran, Central Pamir and

South Afghanistan subterranes. The finding is rather interesting, but we are unsure as to the tectonic feasibility of the proposal. Certainly, though, it could be tested with other techniques.

The basement-age-matching study of Guynn *et al.* (2012, fig. 9) places Sibumasu adjacent to NW Australia, and thus ignores the *c.* 200-km-wide continental shelf here, plus the Exmouth Plateau promontory. Lhasa is draped around western Sibumasu and continues to the western edge of Greater India; Qiangtang is along strike, terminating at the eastern corner of the Arabian block (in Iran; Fig. 19e). Like Ferrari *et al.* (2008), Guynn *et al.* also depict the Iranian block, sitting it off NE Arabia; their suggestion would fit the Alborz Mountain palaeomagnetic data. Although the rifting of these fragments was not a concern of Guynn *et al.* (2012), their positioning of eastern Lhasa–western Sibumasu creates an interesting logic line, appearing to require the two blocks to have departed Gondwana together, or with Lhasa the first to begin its journey to Asia, an idea that is odds with Metcalfe (2011). Unfortunately, Guynn *et al.* do not link Baoshan to the other terranes, nor do they show it in their summary diagram (Guynn *et al.* 2012, fig. 9) but their positioning of both eastern Lhasa and northern Sibumasu accommodate the palaeomagnetic data.

The reconstruction of Dopieralska *et al.* (2012, fig. 5) concludes their paper in which they attempt to deduce the neodymium isotopic composition of sea water during the Late Devonian by way of conodonts preserved in the Sibumasu terrane-rocks in western Thailand. Based on the chemistries, they proposed a correlation with western Australia, and in their GMAP software generated reconstruction they placed Sibumasu 'upside down' in the present-day Perth Basin (Fig. 19f). A fundamental problem with the proposal is block overlap with northern Greater India (see Ali & Aitchison 2005, 2012). Furthermore, they made no attempt to accommodate the other Cimmerian blocks.

Zhu *et al.* (2013, fig. 7) place Qiangtang off northern Greater India (Fig. 19g); Lhasa is directly against northwest Australia. The modelling of both terranes is contentious: Qiangtang would sit atop the Wallaby and Zenith Plateaus, as well as NW Greater India; for Lhasa the reconstruction ignores the wide shelf off Australia and does not consider the compelling evidence that a number of terranes now in SE Asia rifted from the margin 50–60 Myr afterwards in the Late Jurassic (Hall 2011; Metcalfe 2011). Moreover, Sibumasu, which is an integral element in the debate, simply does not feature in their analysis. These issues aside, with the Zhu *et al.* model, the Baoshan data would comfortably fit if the block formed eastern Qiangtang. If eastern Lhasa were the preferred option, the match would be very much marginal.

The modelling of Zhang *et al.* (2013, fig. 5) is based on the patterns of biotic assemblages on the various Gondwana–Cimmeria blocks at key times during the Permian. They place Qiangtang off cratonic India, and Lhasa and Sibumasu adjacent to NW Australia (Fig. 19h). All three terranes show substantial overlap. Additionally, Lhasa and Sibumasu are clearly smaller than their present-day forms. These issues aside, the Baoshan data can just about be accommodated with their model (towards the lower limit of the permissible range).

7.3 Potential for future palaeomagnetism studies to evaluate model proposals

Unfortunately, the palaeomagnetic data set that is available for the Early Permian rocks on the three key blocks is not particularly good. As part of their major compilation Li *et al.* (2004) reported just a single result for Lhasa, five for Qiangtang and none for Sibumasu (if Baoshan, which is inferred to be part of the terrane, is excluded). In all cases (we have examined the original publications) the samples sets are too small and/or the directions have poor cluster statistics—Van der Voo (1990) provides a useful guide. Recently, Cheng *et al.* (2012) and Ran *et al.* (2012) have added to the data set, but the sample sets they provide for Upper Carboniferous through Middle Permian rocks are still small (respectively, seven sites for northern Qiangtang and five sites for Lhasa). Interestingly, however, the obtained directions yield palaeolatitudes around 14–17°S, which in our 280 Ma reconstruction (Figs 18 and 19) would see both blocks located off northern Arabia (and close to the Alborz block). In modern times, such a configuration has never been proposed, and it is difficult to imagine how the intervening terranes (e.g. Central Pamir, South Afghanistan) could be accommodated into such a model. Thus, there is considerable potential for further detailed palaeomagnetic studies resolving the ambiguities related to the site-of-origin of Qiangtang, Lhasa and Sibumasu in the Gondwana supercontinent (see Ali *et al.* 2012). Critically, all three would stretch between 2700 and 4000 km, thus the latitudinal differences between their ends when placed against Gondwana would be palaeomagnetically resolvable. Also, the idea that Baoshan may have been in close proximity to some western Cimmeria blocks (Shi *et al.* 2011) is another suggestion that could be tested.

8 CONCLUSIONS

A palaeomagnetic investigation of the Woniusi Basalts on the Baoshan block generated directional data from five localities (28 cooling units). When combined with the findings of Huang & Opdyke (1991; three localities, 19 lava flows), it results in a mean inclination of 61.0° ($\alpha_{95} = 7.2°$), equating to a formation latitude of 41.9°S (with errors, the range is 34.2–51.2°S). Using the data, we suggest that Baoshan fitted into a longitudinally narrow belt off eastern Gondwana. We confidently assert that Sibumasu lay directly to the east, some distance offshore NW Australia–northern New Guinea. Both Qiangtang and Lhasa almost certainly sat to the west, north of Greater India–SE Arabia but we are unsure of their exact configuration. We note, though, that several somewhat different models can, to varying degrees also accommodate the data. There is much potential for detailed palaeomagnetic studies of Early Permian through Triassic rocks on all three of the eastern Cimmeria subterranes resolving these uncertainties.

ACKNOWLEDGEMENTS

Funding was provided by an award from the Hong Kong Universities' Research Grants Council to JRA (HKU7001/10). We thank Xulong Lai for help with fieldwork logistics, Diane Chung for retrieving and translating some Chinese-language references and Qinglai Feng, Xiaochi Jin and Jiaxin Yan for sharing information. The manuscript's two anonymous reviewers are thanked for their thoughtful, incisive critiques. The study is a contribution to IGCP589: *Development of the Asian Tethyan Realm: Genesis, Process and Outcomes*.

REFERENCES

Aitchison, J.C., Ali, J.R. & Davis, A.M., 2007. When and where did India and Asia collide? *J. geophys Res.,* **112B,** B05423, doi:10.1029/2006JB004706.

Ali, J.R. & Aitchison, J.C., 2005. Greater India, *Earth-Sci. Rev.,* **72,** 169–188.
Ali, J.R. & Aitchison, J.C., 2012. Comment on "Restoration of Cenozoic deformation in Asia and the size of Greater India" by D. J. J. van Hinsbergen *et al.*, *Tectonics,* **31,** doi:10.1029/2011TC003091.
Ali, J.R., Fitton, J.G. & Herzberg, C., 2010. Emeishan large igneous province (SW China) and the mantle plume up-doming hypothesis, *J. Geol. Soc. Lond.,* **167,** 953–959.
Ali, J.R., Aitchison, J.C., Chik, S.Y.S., Baxter, A.T. & Bryan, S.E., 2012. Paleomagnetic data support Early Permian age for the Abor Volcanics in the lower Siang Valley, NE India: significance for Gondwana-related break-up models, *J. Asian Earth Sci.,* **50,** 105–115.
Audley-Charles, M.G., 1983. Reconstruction of eastern Gondwanaland, *Nature,* **306,** 48–50.
Besse, J., Torcq, F., Gallet, Y., Ricou, L.E., Krystyn, L. & Saidi, A., 1998. Late Permian to Late Triassic palaeomagnetic data from Iran: constraints on the migration of the Iranian block through the Tethyan Ocean and initial destruction of Pangaea, *Geophys. J. Int.,* **135,** 77–92.
Burrett, C., Long, J. & Stait, B., 1990. Early-Middle Palaeozoic biogeography of Asian terranes derived from Gondwana, in *Palaeozoic Palaeogeography and Biogeography,* Vol. 12, pp. 163–74, eds McKerrow, W.S. & Scotese, C.R., Geol. Soc. Lond. Mem.
Burrett, C., Duhig, N., Berry, R. & Varne, R., 1991. Asian and Southwestern Pacific continental terranes derived from Gondwana, and their biogeographic significance, *Aust. J. System. Bot.,* **4,** 13–24.
Cheng, X. *et al.*, 2012. Paleomagnetic results of Late Paleozoic rocks from northern Qiangtang Block in Qinghai-Tibet Plateau, China, *Sci. China Earth Sci.,* **55,** 67–75.
Colwell, J.B., Symonds, P.A. & Crawford, A.J., 1994. The nature of the Wallaby (Cuvier) Plateau and other igneous provinces of the west Australian margin, *AGSO J. Aust. Geol. Geophys.,* **15,** 137–156.
Dopieralska, J., Belka, Z., Königshof, P., Racki, G., Savage, N., Lutat, P. & Sardsud, A., 2012. Nd isotopic composition of Late Devonian seawater in western Thailand: geotectonic implications for the origin of the Sibumasu terrane, *Gondwana Res.,* **22,** 1102–1109.
Ferrari, O.M., Hochard, C. & Stampfli, G.M., 2008. An alternative plate tectonic model for the Palaeozoic–Early Mesozoic Palaeotethyan evolution of Southeast Asia (Northern Thailand–Burma), *Tectonophysics,* **451,** 346–365.
Fisher, R.A., 1953. Dispersion on a sphere, *Proc. R. Soc. Lond.,* **A217,** 295–305.
Gehrels, G. *et al.*, 2011. Detrital zircon geochronology of pre-Tertiary strata in the Tibetan-Himalayan orogen, *Tectonics,* **30,** TC5016, doi:10.1029/2011TC002868.
Gradstein, F.M. *et al.*, 2005. *A Geologic Time Scale 2004,* Cambridge University Press, Cambridge, 589 p.
Guynn, J., Kapp, P., Gehrels, G.E. & Ding, L., 2012. U–Pb geochronology of basement rocks in central Tibet and paleogeographic implications, *J. Asian Earth Sci.,* **43,** 23–50.
Hall, R., 2011. Australia–SE Asia collision: plate tectonics and crustal flow, in *The SE Asian Gateway: History and Tectonics of the Australia–Asia Collision,* Vol. 355, pp. 75–109, eds Hall, R., Cottam, M.A. & Wilson, M.E.J., Geol. Soc. Lond. Spec. Pub.
Huang, K.N. & Opdyke, N.D., 1991. Paleomagnetic results from the Upper Carboniferous of the Shan-Thai-Malay block of western Yunnan, China, *Tectonophysics,* **192,** 333–344.
Jaeger, J.J., Courtillot, V. & Tapponnier, P., 1989. Paleontological view of the ages of the Deccan Traps, the Cretaceous/Tertiary boundary, and the India-Asia collision, *Geology,* **17,** 316–319.
Jin, X.C., 2002. Permo-Carboniferous depositional sequences of Gondwana affinity in southwest China and their paleogeographic implications, *J. Asian Earth Sci.,* **20,** 633–646.
Jian, P., Liu, D.Y., Kröner, A., Zhang, Q., Wang, Y.Z., Sun, X.M. & Zhang, W., 2009. Devonian to Permian plate tectonic cycle of the Paleo-Tethys Orogen in southwest China (I): geochemistry of ophiolites, arc/back-arc assemblages and within-plate igneous rocks, *Lithos,* **113,** 748–766.
Kirschvink, J.L., 1980. The least squares line and plane and the analysis of paleomagnetic data, *Geophys. J. R. astr. Soc.,* **62,** 699–718.
Kondo, K., Mu, C.L., Yamamoto, T., Zaman, H., Miura, D., Yokoyama, M., Ahn, H.S. & Otofuji, Y., 2012. Oroclinal origin of the Simao Arc in the Shan-Thai Block inferred from the Cretaceous palaeomagnetic data, *Geophys. J. Int.,* **190,** 201–216.
Leloup, P.H. *et al.*, 1995. The Ailao Shan–Red River shear zone (Yunnan, China), Tertiary transform boundary of Indochina, *Tectonophysics,* **251,** 3–84.
Li, P.W., Gao, R., Cui, J. & Guan, Y., 2004. Paleomagnetic analysis of eastern Tibet: implications for the collisional and amalgamation history of the Three Rivers Region, SW China, *J. Asian Earth Sci.,* **24,** 291–310.
McFadden, P.L. & Reid, A.B., 1982. Analysis of palaeomagnetic inclination data, *Geophys. J. R. astr. Soc.,* **69,** 307–319.
Metcalfe, I., 1996. Pre-Cretaceous evolution of SE Asian terranes, in *Tectonic Evolution of Southeast Asia,* Vol. 106 pp. 97–122, eds Hall, R. & Blundell, D., Geol. Soc. Lond. Spec. Pub.
Metcalfe, I., 1998. Palaeozoic and Mesozoic geological evolution of the SE Asian region: multidisciplinary constraints and implications for biogeography, in *Biogeography and Geological Evolution of SE Asia,* pp. 25–41, eds Hall, R. & Holloway, J.D., Backhuys Publishers, Amsterdam, The Netherlands.
Metcalfe, I., 2002. Permian tectonic framework and palaeogeography of SE Asia, *J. Asian Earth Sci.,* **20,** 551–566.
Metcalfe, I., 2011. Tectonic framework and Phanerozoic evolution of Sundaland, *Gondwana Res.,* **19,** 3–21.
Moix, P., Beccaletto, L., Kozur, H.W., Hochard, C., Rosselet, F. & Stampfli, G.M., 2008. A new classification of the Turkish terranes and sutures and its implication for the paleotectonic history of the region, *Tectonophysics,* **451,** 7–39.
Molnar, P. & Tapponnier, P., 1975. Cenozoic tectonics of Asia: effects of a continental collision, *Science,* **189,** 419–426.
Muttoni, G. *et al.*, 2009. Opening of the Neo-Tethys Ocean and the Pangea B to Pangea A transformation during the Permian, *GeoArabia,* **14**(4), 17–44.
Nie, S.Y, Rowley, D.B. & Ziegler, A.M., 1990. Constraints on the locations of Asian microcontinents in Palaeo-Tethys during the Late Palaeozoic, in *Palaeozoic Palaeogeography and Biogeography,* Vol. 12, pp. 397–409, eds McKerrow, W.S. & Scotese, C.R., Geol. Soc. Lond. Mem.
Otofuji, Y., Yokoyama, M., Kitada, K. & Zaman, H., 2010. Paleomagnetic versus GPS determined tectonic rotation around eastern Himalayan syntaxis in East Asia, *J. Asian Earth Sci.,* **37,** 438–451.
Patriat, P. & Achache, J., 1984. India-Eurasia collision chronology has implications for crustal shortening and driving mechanism of plates, *Nature,* **311,** 615–621.
Ran, B., Wang, C.S., Zhao, X.X., Li, Y.L., He, M., Zhu, L.D., Coe, R.S. & Lippert, P.C., 2012. New paleomagnetic results of the Early Permian in the Xainza area, Tibetan Plateau and their paleogeographical implications, *Gondwana Res.,* **22,** 447–460.
Ridd, M.F., 1971. Southeast Asia as a part of Gondwanaland, *Nature,* **234,** 531–533.
Ridd, M.F., 2009. The Phuket Terrane: a Late Palaeozoic rift at the margin of Sibumasu, *J. Asian Earth Sci.,* **36,** 238–251.
Şengör, A.M.C., Yilmaz, Y. & Ketin, I., 1980. Remnants of a pre-Late Jurassic ocean in northern Turkey: fragments of Permian-Triassic Paleo-Tethys? *Geol. Soc. Am. Bull.,* **91,** 599–609.
Şengör, A.M.C., Altmer, D., Cin, A., Ustaömer, T. & Hsü, J.J., 1988. Origin and assembly of the Tethyside orogenic collage at the expense of Gondwanaland, in *Gondwana and Tethys,* Vol. 37, pp. 119–181, eds Audley-Charles, M.G. & Hallam, A., Geol. Soc. Lond. Spec. Pub.
Shi, G.R., 2003. Aspects of Permian Gondwana in central Tibet and SE Asia: distribution, paleoclimatic and paleogeographical implications, in *Proceedings of the XVth International Congress on Carboniferous and Permian Stratigraphy,* ed. Wong, T.E., 10–16 August 2003, Royal Netherlands Academy of Arts and Sciences, Utrecht, the Netherlands, pp. 555–564.
Shi, Y.K., Huang, H., Jin, X.C. & Yang, X.N., 2011. Early Permian fusulinids from the Baoshan block, western Yunnan, China and their paleobiogeographic significance, *J. Paleont.,* **85**(2011), 489–501.
Smith, A.G. & Hallam, A., 1970. The fit of the southern continents, *Nature,* **225,** 139–144.

Socquet, A. & Pubellier, M., 2005. Cenozoic deformation in western Yunnan (China–Myanmar border), *J. Asian Earth Sci.,* **24,** 495–515.

Stampfli, G.M., Borel, G.D., Cavazza, W., Mosar, J. & Ziegler, P.A., 2001. Palaeotectonic and palaeogeographic evolution of the western Tethys and PeriTethyan domain (IGCP Project 369), *Episodes,* **24,** 22–28.

Stilwell, J.D., Quilty, P.G. & Mantle, D.J., 2012. Paleontology of Early Cretaceous deep-water samples dredged from the Wallaby Plateau: new perspectives of Gondwana break-up along the Western Australian margin, *Austr. J. Earth Sci.,* **59,** 29–49.

Tapponnier, P., Peltzer, G., Le Dain, A.Y., Armijo, R. & Cobbold, P., 1982. Propagating extrusion tectonics in Asia: new insights from simple experiments with plasticine, *Geology,* **10,** 611– 616.

Torsvik, T.H. & Smethurst, M.A., 1999. Plate tectonic modelling: virtual reality with GMAP, *Comp. Geosci.,* **25,** 395–402.

Torsvik, T.H., Müller, R.D., Van der Voo, R., Steinberger, B. & Gaina, C., 2008. Global plate motion frames: toward a unified model, *Rev. Geophys.,* **46,** doi:10.1029/2007RG000227.

Ueno, K., 2003. The Permian fusulinoidean faunas of the Sibumasu and Baoshan blocks: their implications for the paleogeographic and paleoclimatologic reconstruction of the Cimmerian Continent, *Palaeogeogr. Palaeoclimat. Palaeoecol.,* **193,** 1–24.

Van der Voo, R., 1990. The reliability of paleomagnetic data, *Tectonophysics,* **184,** 1–9.

Veevers, J.J. & Tewari, R.C., 1995. Permian– Carboniferous and Permian–Triassic magmatism in the rift zone bordering the Tethyan margin of southern Pangea, *Geology,* **23,** 467–470.

Wang, X.L., Kato, M. & Wang, H.Z., 1996. On the tectonic position of the Baoshan region during the Late Palaeozoic, *J. Southeast Asian Earth Sci.,* **13,** 171–183.

Wang, E., Burchfiel, B.C., Royden, L.H., Chen, L., Chen, J., Li, W. & Chen, Z., 1998. Late Cenozoioc Xianshuihe-Xiaojiang, Red River, and Dali Fault systems of southwestern Sichuan and central Yunnan, China, *Geol. Soc. Am. Spec. Pap.,* **327,** 108p.

Wang, X.D., Ueno, K., Mizuno, Y. & Sugiyama, T., 2001. Late Paleozoic faunal, climatic, and geographic changes in the Baoshan Block as a Gondwana-derived continental fragment in Southwest China, *Palaeogeogr. Palaeoclimat. Palaeoecol.,* **193**(170), 197–218.

Wang, W., Dong, Z. & Wang, C., 2004. The conodont ages of the Dingjiazhai and Woniusi Formations in the Baoshan Area, Western Yunnan, *Acta Micropal. Sinica,* **21,** 273–282.

Wensink, H., 1979. The implications of some paleomagnetic data from Iran for its structural history, *Geologie en Mijnbouw,* **58,** 175–185.

Wopfner, H., 1996. Gondwana origin of the Baoshan and Tengchong terranes of west Yunnan, in *Tectonic Evolution of Southeast Asia,* Vol. 106, pp. 539–547, eds Hall, R. & Blundell, D., Geol. Soc. Lond. Spec. Pub.

Wopfner, H. & Jin, X.C., 2009. Pangea megasequences of Tethyan Gondwana-margin reflect global changes of climate and tectonism in Late Palaeozoic and Early Triassic times: a review, *Palaeoworld,* **18,** 169–192.

Yamashita, I., Surinkum, A., Wada, Y., Fujihara, M., Yokoyama, M., Zaman, H. & Otofuji, Y., 2011. Paleomagnetism of the Middle–Late Jurassic to Cretaceous red beds from the Peninsular Thailand: implications for collision tectonics, *J. Asian Earth Sci.,* **40,** 784–796.

Yan, J.X. & Yin, H.F., 2000. Paleoclimatic constraints for Early Permian paleogeography of eastern Tethys, in *Permian-Triassic Evolution of Tethys and Western Circum-Pacific,* pp. 1–15, eds Yin, H., Dickins, G.M., Shi, G.R. & Tong, J., Elsevier.

Yan, J.X. & Zhao, K., 2001. Permo-Triassic paleogeographic, paleoclimatic and paleoceanographic evolutions in eastern Tethys and their coupling, *Sci. China Ser. D Earth Sci.,* **44,** 968–978.

Yan, J.X., Liang, D.Y. & Wu, M., 2004. Permian carbonates of Baoshan block, western Yunnan and their paleoclimatic implications, *Sci. China Ser. D Earth Sci.,* **47,** 385–392.

Zhang, Y.C., Shi, G.R. & Shen, S.Z., 2013. A review of Permian stratigraphy, palaeobiogeography and palaeogeography of the Qinghai-Tibet Plateau, *Gondwana Res.,* **23,** doi:10.1016/j.gr.2012.06.010.

Zhu, D.C., Zhao, Z.D., Niu, Y.L., Dilek, Y., Wang, L.Q. & Mo, X.X., 2011. Lhasa Terrane in southern Tibet came from Australia, *Geology,* **39,** 727–730.

Zhu, D.C., Zhao, Z.D., Niu, Y.L., Dilek, Y., Hou, Z.Q. & Mo, X.X., 2013. The origin and pre-Cenozoic evolution of the Tibetan Plateau, *Gondwana Res.,* **23,** doi:10.1016/j.gr.2012.02.002.

Zijderveld, J.D.A., 1967. A.C. demagnetization of rocks, in *Methods in Paleomagnetism,* pp. 256–286, eds Collinson, D.W., Creer, K.M. & Runcorn, S.K., Elsevier, New York.